Mapping metastability of Lennard-Jones clusters by maximum vibrational frequency

Shota Ono *

Department of Electrical, Electronic and Computer Engineering, Gifu University, Gifu 501-1193, Japan

(Received 26 November 2021; revised 22 March 2022; accepted 31 March 2022; published 11 April 2022)

We study the structure-stability relationship of Lennard-Jones (LJ) clusters from a point of view of vibrations. By assuming the size up to $N = 1610$, we demonstrate that the N dependence of the maximum vibrational frequency reflects the geometry of the core (the interior of a cluster) that will determine the overall geometry of the cluster. This allows us to identify the formation of nonicosahedral structures for $N \leqslant 150$, the vacancy formation at the core for $N \geqslant 752$, and the transition from icosahedral to decahedral structures at $N = 1034$. We apply the maximum frequency analysis to classify metastable clusters for $19 \leqslant N \leqslant 39$, where transformation pathways between different structures are visualized, and the energy barrier height is estimated simultaneously.

DOI: 10.1103/PhysRevB.105.134104

I. INTRODUCTION

Assembly of atoms constitutes nanoclusters, and the structure, thermodynamics, and growth process have been extensively investigated for many elemental systems such as Pb [1–3], Ni [4], Au [5,6], and transition metals [7,8] (see also Ref. [9] for a review). The number of atoms N plays an important role in understanding the stability of clusters because the total energy at a specific N is particularly low, compared to that at $N \pm 1$. In addition, the cluster geometry can be highly symmetric. For example, the clusters at $N = 13$ and 55 can have relatively small energy, which is usually attributed to the icosahedral geometry. On the other hand, for large N, the structure of clusters is determined by several factors (i.e., the volume, surface, edges, and vertices of clusters), and the geometry changes from the icosahedral to decahedral to face-centered cubic (fcc) structures as N increases [9]. Recently, the clusters with the decahedral structure have been created for several noble metals [10], which has attracted attention due to their optical and catalytic properties that are different from those with the icosahedral structure.

The stability and geometry of the Lennard-Jones (LJ) clusters have been extensively studied for many years [11–27]. It has been known that the $N = 13$ icosahedron serves as a seed to generate the lowest energy atomic configurations [20], that is, the LJ clusters for $N \geqslant 13$ have an icosahedron at the core surrounded by the surface atoms. However, for the cases of $N = 38$, 75–77, 98, and 102–104, the core of the LJ clusters has octahedral, decahedral, tetrahedral, and decahedral structures, respectively [15,16,20]. Even when the energetic stability analyses are employed, no significant anomalies have been found at these Ns. In general, the cluster geometry is characterized by studying the local atomic environment in detail, as done by Polak and Patrykiejew [21] and Yang and Tang [27], where they used four structural motifs (fcc, hcp, icosahedral, and decahedral) to understand the overall and core geometries. Alternatively, we expect that the lattice dynamics calculations might be useful to understand the core geometry because the normal modes at the maximum frequency will involve the vibration of the most rigid part (i.e., the core) in the system. For example, the sequence of the maximum frequency as a function of N should identify the difference of the core geometries in the LJ clusters.

In this paper, we study the energetic and vibrational properties of LJ clusters up to $N = 1610$. The N dependence of the maximum frequency allows us to identify the core geometry that is different from the icosahedral structure. It also enables us to identify the vacancy formation at the core and the structural transition from icosahedra to decahedra for large N. As another application, we construct a metastability map, where the maximum frequency is plotted as the total energy for many metastable structures. For the cases of $19 \leqslant N \leqslant 39$, we distinguish the clusters with decahedra from those with icosahedra. In addition, we identify transformation pathways between different structures, and estimate the energy barrier height. The present work will pave the way to understand the structural stability and geometry based on the vibrational frequency.

The vibrational frequency analysis has been recently applied to study the magic numbers in N charges on a sphere [28], while finding the lowest energy configurations on a sphere is known as the Thomson problem. The maximum frequency showed relatively small values at $N = 12$, 32, 72, 132, 192, 212, 272, 282, and 372. The presence of these magic numbers reflects both the charge configurations on a sphere and the strong degeneracy of the one-particle energies. In contrast, the LJ particles that we study in the present work are free from the boundary condition, and therefore the core geometry of the system influences the vibrational properties. Doye and Calvo have calculated the geometric mean vibrational frequency of the LJ clusters to distinguish the nonicosahedral structures from the icosahedral structure at the selected sizes of $N = 38$, 75, 98, and 102 [19]. Calvo *et al.* have estimated the Debye temperature of the LJ clusters by fitting the heat capacity, where nonmonotonic behavior in

*shota_o@gifu-u.ac.jp

 ©2022 American Physical Society

the Debye temperature for small $N < 100$ was suggested [18]. The maximum frequency that we use in the present work is directly related to the vibration of the core around which the interatomic bonding is the strongest in the cluster.

Our approach can provide a useful insight of the structure-stability relationship among metastable structures as well, only by performing the maximum frequency and total energy calculations. The metastability of nanoclusters has been studied by calculating the potential energy surface (PES) and/or constructing the disconnectivity graph [29]. These approaches are useful to understand the relationship between the energetic stability and the structure of nanoclusters, which has been applied to predict the synthesizability of nanostructures [30,31]. However, visualizing the PES is not straightforward [32]: among $3N$ degrees of freedom one must find a few parameters describing the transformation between different structures. To construct the disconnectivity graph, one must find the transition states having one imaginary frequency mode.

II. THEORY

We study the dynamics of the LJ clusters having N atoms within the harmonic approximation. The equations of motion can be written as [33,34]

$$m\frac{d^2u_{i\alpha}}{dt^2} = -\sum_{j\beta} D^{ij}_{\alpha\beta}u_{j\beta}, \tag{1}$$

where $u_{i\alpha}$ is the displacement along α direction for the particle i with a mass of m. The force constant matrix $D^{ij}_{\alpha\beta}$ is defined as

$$D^{ij}_{\alpha\beta} = D^{ji}_{\beta\alpha} = \left.\frac{\partial^2 E}{\partial R_{i\alpha}\partial R_{j\beta}}\right|_0, \tag{2}$$

where the derivative is taken at the equilibrium configurations. E is the total potential energy

$$E = \sum_{i=1}^{N} \varepsilon_i \tag{3}$$

with the one-particle energy

$$\varepsilon_i = \frac{1}{2}\sum_{j\neq i} 4A\left[\left(\frac{\sigma}{r_{ij}}\right)^{12} - \left(\frac{\sigma}{r_{ij}}\right)^{6}\right], \tag{4}$$

where $1/2$ accounts for the double counting of the interaction energy, A and σ are parameters of the LJ potential, and r_{ij} is the interparticle distance between the LJ particles i and j, which can be expressed by

$$r^2_{ij} = \sum_{\alpha=x,y,z} (R_{i\alpha} - R_{j\alpha})^2, \tag{5}$$

where $R_{i\alpha}$ is the α component of the position of the particle i. Assuming a stationary solution $u_{i\alpha}(t) = \epsilon_{i\alpha}e^{i\omega t}$ with the frequency ω and the polarization $\epsilon_{i\alpha}$, one obtains the eigenvalue equation

$$m\omega^2\epsilon_{i\alpha} = \sum_{j\beta} D^{ij}_{\alpha\beta}\epsilon_{j\beta}. \tag{6}$$

The stable structure with N particles has $3N - 6$ vibrational modes, where the degrees of freedom for translation and rotation are subtracted. The maximum eigenvalue gives the maximum frequency $\omega_{\max}$. The units of energy and frequency are A and $A^{1/2}\sigma^{-1}m^{-1/2}$, respectively. Throughout the paper, we set $A = \sigma = m = 1$.

To find the lowest energy structures, we referred to two databases. For $3 \leqslant N \leqslant 150$, we referred to the Cambridge Cluster Database (CCD) [35], and for large N up to 1610, we referred to the database provided by Shao *et al.* [36] (310 to 561 atoms [22], 562 to 1000 atoms [23], and 1001 to 1610 atoms [25]). We used the Broyden-Fletcher-Goldfarb-Shanno algorithm [37] to find the local minimum structures for the cases of $N = 19$-39, where the initial positions of N atoms were given by random numbers. For each N, we generated more than 3×10^4 initial configurations and optimized their structures, from which the 2000 lowest energy structures were extracted. In particular, for $N = 31$, 33, and 35, 6×10^4 initial configurations were needed to obtain the lowest energy structures stored at the CCD [35]. However, we failed to find the lowest energy structure at $N = 38$.

To compare the optimized E/N and $\omega_{\max}$ with the bulk values (i.e., the case of $N \to \infty$), we calculated the total energy and the phonon dispersions of the LJ crystal in the fcc structure. The computational details are the same as those described in Ref. [38], while A and σ were set to be unity in the present work. We obtained $E^{\rm fcc}_{\min}/N = -8.609$ and $\omega^{\rm fcc}_{\max} = 28.18$ that corresponds to the longitudinal phonon frequency at the X point in the Brillouin zone.

III. RESULTS AND DISCUSSION

A. Lowest energy structures

Figure 1(a) shows the N dependence of the lowest energy per particle $E_{\min}/N$. The $E_{\min}$ decreases with N, while some dips can be observed at $N = 13$ and 55. At these Ns complete icosahedral structure can be formed [14,20]. To emphasize the magic numbers, at which the N cluster is relatively stable compared to $N \pm 1$ clusters, we define the first and second differences in the total energy as [9]

$$\Delta E = E_{\min}(N-1) - E_{\min}(N), \tag{7}$$

$$\Delta^2 E = E_{\min}(N-1) + E_{\min}(N+1) - 2E_{\min}(N). \tag{8}$$

Figures 1(b) and 1(c) show the N dependence of ΔE and $\Delta^2 E$, respectively. Peaks in $\Delta^2 E$ are observed at several Ns. For example, $N = 13$, 55, and 144 are clearly identified as the magic numbers, where $N = 144$ cluster has also complete icosahedral structure. The relative stability between different Ns can thus be identified by studying ΔE and/or $\Delta^2 E$.

To shed light on another aspect on the LJ cluster properties, we show the N dependence of $\omega_{\max}$ in Fig. 1(d). The value of $\omega_{\max}$ increases with N. However, an anomalous decrease in $\omega_{\max}$ is observed at $N = 38$,75–77, 98, and 102–104. It should be noted that the lowest energy structures at these Ns do not have icosahedra at the core [15,16,20,35]. This shows that the atomic displacement of the maximum frequency mode reflects the core geometry. For the $N = 55$ cluster having an icosahedron at the core, the displacement localizes to the core atom. On the other hand, $N = 38$ and 75 clusters has an octahedron and a decahedron at the core, and the

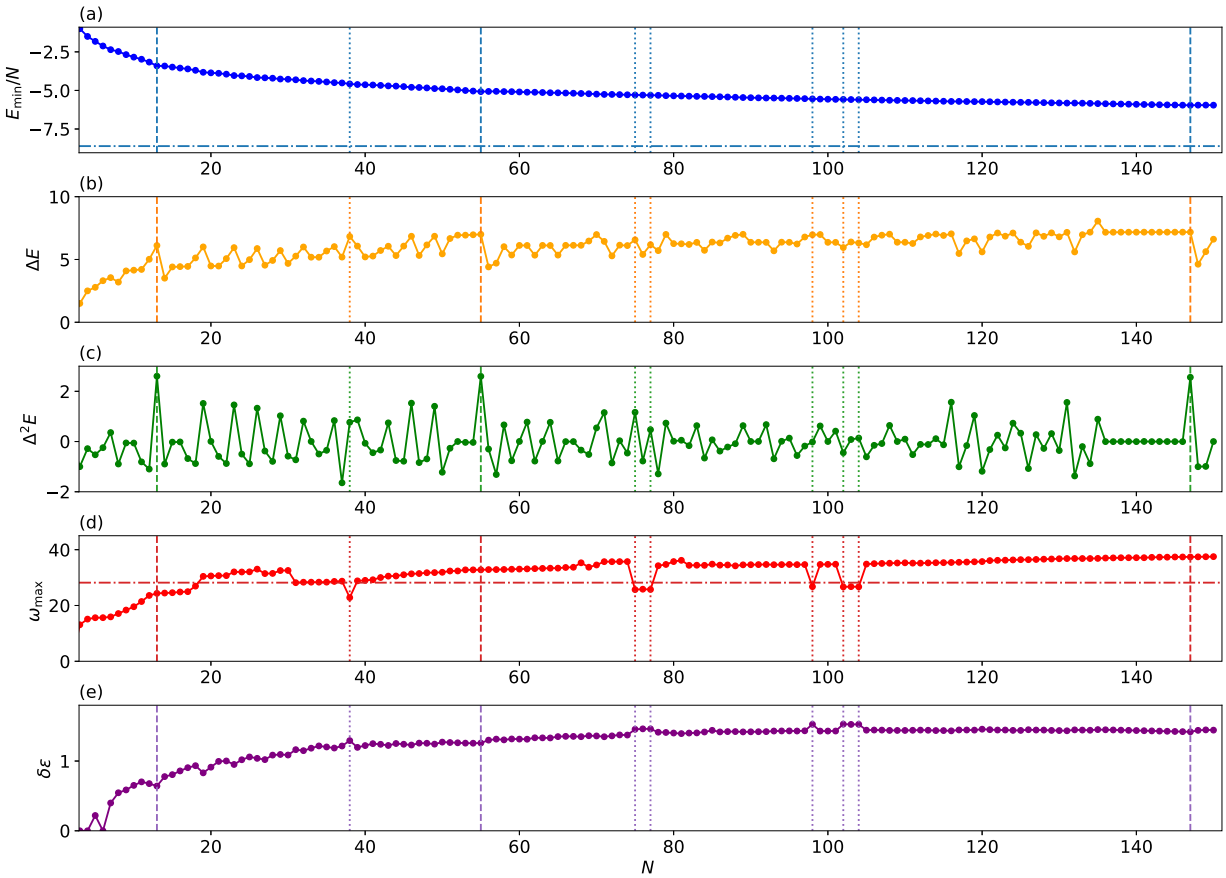

FIG. 1. The N dependence of (a) $E_{\min}/N$, (b) ΔE, (c) $\Delta^2 E$, (d) $\omega_{\max}$, and (e) $\delta\varepsilon$. The vertical dashed lines indicate $N = 13,\ 55$, and 147 (complete icosahedral structure). The vertical dotted lines indicate $N = 38,\ 75,\ 77,\ 98,\ 102$, and 104 (nonicosahedral structure). The horizontal dot-dashed lines in (a) and (d) indicate the values for the fcc structure.

displacement pattern is a breathing of the octahedron for $N = 38$ and asymmetric displacements along the five-fold symmetric axis for $N = 75$, as shown in Fig. 2. The maximum frequency mode for the $N = 76$, 77, and 102–104 clusters is similar to that for the $N = 75$ cluster: the core at $N =$ 102–104 has 19 atoms forming a one-dimensional tube of three decahedra with the five-fold rotational symmetry, and the displacement pattern shows the expansion, contraction, and expansion of the three decahedra. The $N = 98$ cluster has a large core with tetrahedral shape [16], and the displacement localizes to this core in a complicated manner. In this way, the analysis of the N dependence of $\omega_{\max}$ allows us to distinguish the core geometry from icosahedra.

The difference of the core geometry as well as the decrease in $\omega_{\max}$ are related to the distribution of ε_i in Eq. (4). In general, the ε_i of the core atom i is lower than that of the surface atoms because the interatomic bonding strength as well as the coordination number will be large around the core, unless the vacancy formation occurs at the core for relatively large N [24]. The values of ε_i are thus scattered as N increases because the core and surface regions are clearly separated for large N. The distribution of ε_i will be modified when the geometry of the core changes. Figure 1(e) shows the standard deviation $\delta\varepsilon$ of ε_i as a function of N. The peaks in $\delta\varepsilon$ are well correlated to the decrease in $\omega_{\max}$ in Fig. 1(d).

The increase in $\delta\varepsilon$ can be visualized by the density-of-states (DOS) for ε_i shown in Fig. 3, where the DOS of the lowest energy (nonicosahedral) structure and the local minimum (icosahedral) structure (extracted from the CCD [35]) are shown for $N = 38$, 75–77, 98, and 102–104. The gaussian broadening method is applied, and the DOS is shifted depending on the N. The DOS peaks observed for the lowest energy structure are smeared out or split when the icosahedral structure (a local minima) is considered. The value of ε_i and the degeneracy for the $N = 38$ are listed in Table I.

TABLE I. The values of ε_i with $i = 1$ to 7 for several Ns. The figure in parenthesis indicates the degeneracy. The "38g" and "38i" indicate the global minimum and the icosahedral structure at $N = 38$, respectively.

N	ε_1	ε_2	ε_3	ε_4	ε_5	ε_6	ε_7	ε_8	ε_9
38g	−7.146 (6)	−5.338 (8)	−3.681 (24)	-	-	-	-	-	
38i	−7.208 (1)	−6.900 (5)	−6.003 (1)	−4.795 (5)	−4.713 (5)	−4.274 (5)	−3.584 (10)	−3.540 (1)	−3.450 (5)

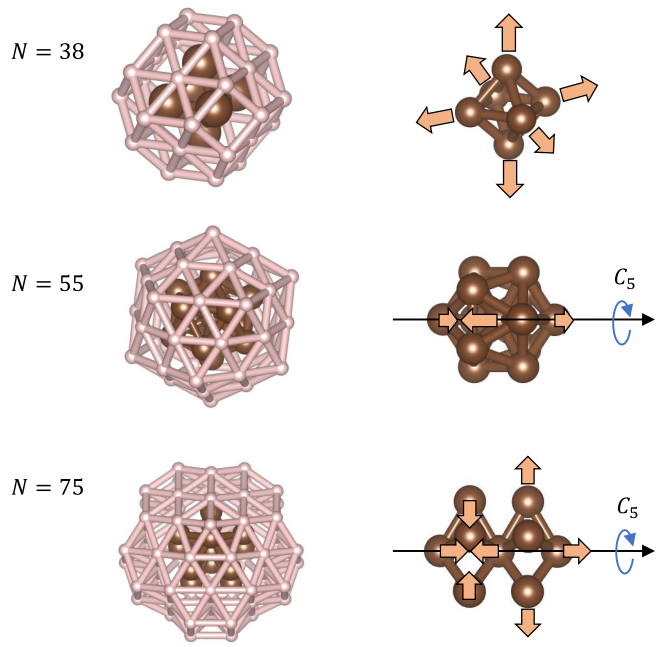

FIG. 2. The structure of the lowest energy atomic configurations (left) and the displacement vectors of the maximum frequency mode (right) for $N = 38$, 55, and 75. The atoms at the core region are colored brown. The core at $N = 55$ and 75 has the five-fold rotational symmetry. One out of three degenerated modes is shown for $N = 55$.

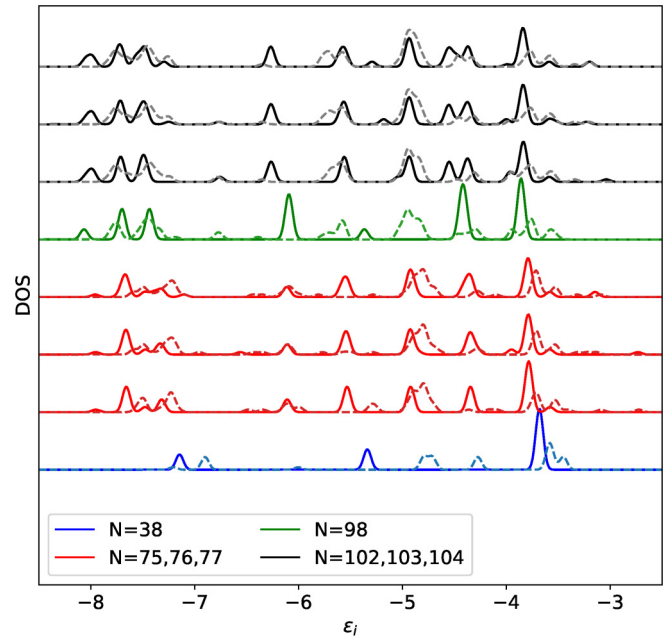

FIG. 3. The one-particle DOS for $N = 38$, 75, 76, 77, 98, 102, 103, and 104 clusters in the lowest energy structure (solid) and in the icosahedral structure (dashed).

As shown in Fig. 1(a), the $E_{\min}/N$ approaches the $E_{\min}^{\mathrm{fcc}}/N$ as N increases. However, the energy difference is still large: $E_{\min}/N = -5.955$ for $N = 150$, and the relative error is more than 30%. When N is increased up to 1610, $E_{\min}/N = -7.338$ [25], and the error is reduced to 15%. It is interesting to study how the $\omega_{\max}$ approaches the bulk value of $\omega_{\max}^{\mathrm{fcc}}$ because the N dependence of $\omega_{\max}$ is nonmonotonic for small N, as shown in Fig. 1(d). In addition, Shao *et al.* have proposed the vacancy formation at the core for $N \geqslant 752$ [24] and the structural transition from icosahedra to decahedra at $N = 1034$ [25], which will influence the N dependence of $\omega_{\max}$. Figure 4 shows the $\omega_{\max}$ as a function of N up to 1610: (i) The $\omega_{\max}$ increases from 37 to 43 for $151 \leqslant N \lesssim 600$, except for $188 \leqslant N \leqslant 192$ and $236 \leqslant N \leqslant 238$; (ii) the value of $\omega_{\max}$ decreases to 35 around $N \simeq 600$, deviates around 35 for $600 \lesssim N \lesssim 800$, and increases from 35 to 36 for $800 \lesssim N \leqslant 1034$; and (iii) the $\omega_{\max}$ shows a sudden drop to 29 at $N = 1035$, and almost keeps the constant value of 29 up to $N = 1610$, while the jump within $1367 \leqslant N \leqslant 1422$ is observed.

The property (i), an increase in $\omega_{\max}$ with N, indicates the hardening of the core in the cluster, which is also observed in small N [see Fig. 1(d)]. The property (ii), an significant decrease in $\omega_{\max}$ from 43 to 35, reflects the vacancy formation at the core: for $N \geqslant 752$, the icosahedral structures with the central vacancy are more stable except for $N = 923$ [24]. We consider that some of the peaks around $600 \lesssim N \lesssim 800$ and $N = 923$ will be a reminiscence of the behavior for $N \lesssim 600$. The property (iii) indicates the transition from the icosahedral to decahedral structures [25]. The jump of $\omega_{\max}$ within $1367 \leqslant N \leqslant 1422$ is also consistent with the formation of the icosahedral structure with the central vacancy at $N = 1402$ [25]. In this sense, the anomalous decreases around $188 \leqslant N \leqslant 192$, $236 \leqslant N \leqslant 238$, $650 \leqslant N \leqslant 664$, $682 \leqslant N \leqslant 689$, $755 \leqslant N \leqslant 762$, and $815 \leqslant N \leqslant 823$ can be attributed to the formation of the decahedral structure. The decahedral and icosahedral structures for the selected Ns are shown in Fig. 4.

It should be noted that the N dependence of $\omega_{\max}$ is strongly correlated with that of the fcc motif concentration. Yang and Tang studied how many structural motifs are there in the LJ cluster for each N by considering four types of motifs in the fcc, hcp, icosahedral, and decahedral structures with 13 atoms, and showed that the fcc motif concentration is relatively large when $N = 38$, 75–78, 102–104, 188–192, 236–238, and $N \simeq 1030$ [27]. They attributed such an enhancement to the formation of the Marks decahedron rather than the Mackay icosahedron, which is consistent with our characterization in geometry.

B. Metastable structures

We next apply the $\omega_{\max}$-based analysis to a classification of the metastable structures with N fixed. Figure 5 shows the distribution of $\omega_{\max}$ as a function of E for the case of $N = 19$, where the 2000 lowest energy structures are plotted. Data points form an island in the E-$\omega_{\max}$ plane, which enables us to classify metastable structures into some groups. The lowest energy structure (group 1) is a barrel-shaped double icosahedron, where four atoms form the symmetry axis along which three pentagons are stacked with twisted angle of $\pi/5$. The structures of other groups are basically derived from the group 1 structure (see Fig. 5): in the second lowest energy structure (group 2), the vertex located on the symmetry axis moves to another facet; in the group 3 and 4 structures, the vertex on the first (or third) and second layer of the pentagon

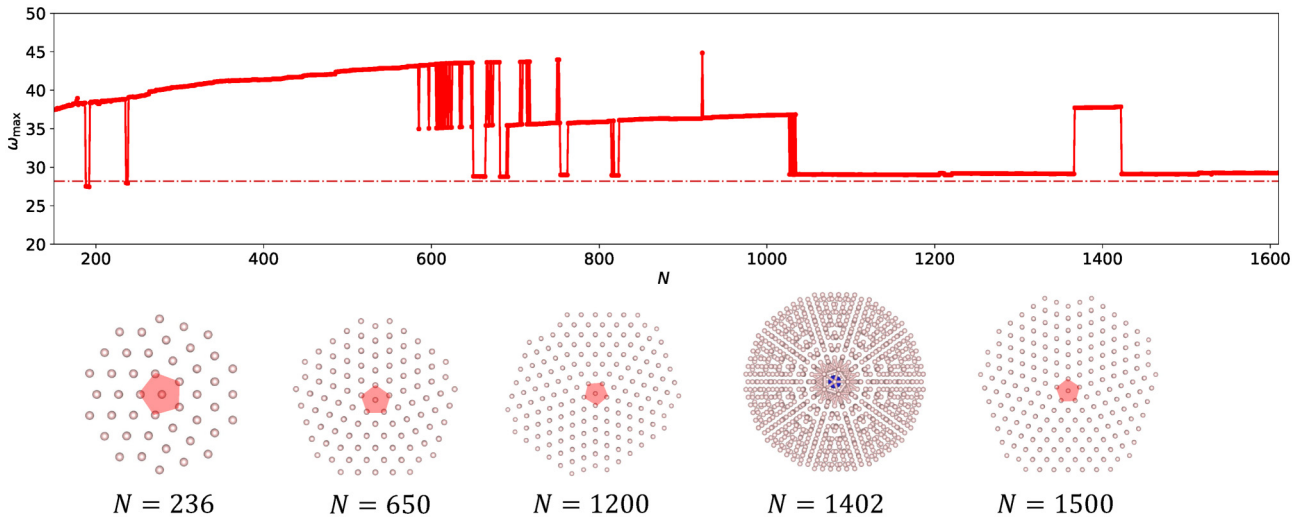

FIG. 4. The N dependence of ω_{max} for the lowest energy structures: $151 \leqslant N \leqslant 1610$. The dot-dashed line indicates the ω_{max}^{fcc}. The four clusters with the decahedral structure (colored red) are shown. The $N = 1402$ cluster with the icosahedral structure is also shown, where the central vacancy is colored blue and the interatomic bonding is illustrated for $r_{ij} \leqslant 1.05\sigma$.

moves to another facet, respectively; and in the group 5 structures, two vertices moves to other facets. As one approaches the continent (i.e., densely plotted region for $E \geqslant -69$), the structures with more complex geometry are observed.

One can find three anomalous structures, which are apart from the continent, with $-70 \leqslant E \leqslant -69$ and relatively small values of ω_{max} ($\simeq$20.8). As depicted in Fig. 5, those metastable structures (group 6) have a decahedron at the core. This result also confirms that the clusters with nonicosahedra can have relatively small ω_{max}.

We also found that some of the structures have a decahedron: For example, those structures have $(E, \omega_{max}) = (-68.9578, 20.81)$ and $(-68.6245, 20.92)$. Among the 2000 structures generated in the present calculations, the 142th structure ($E = -68.8976$) has the lowest maximum frequency of $\omega_{max} = 19.77$, but has neither a decahedron nor an icosahedron at the core region (see group 7 in Fig. 5).

We assume that a structural transformation of clusters may occur between similar geometries, and completely different geometry will be obtained through transformations several times. In this sense, the E-ω_{max} map gives a rough estimation of the energy barrier height between different structures. For example, the transformation from the group 1 to group 2 can be possible when the energy about $2A$ is added. On the other hand, to obtain the clusters with the decahedral structures, the structure in the group 1 must first move to the continent around $E \geqslant -68$ (containing geometries that are potentially transformed into a decahedron), and next moves to the island

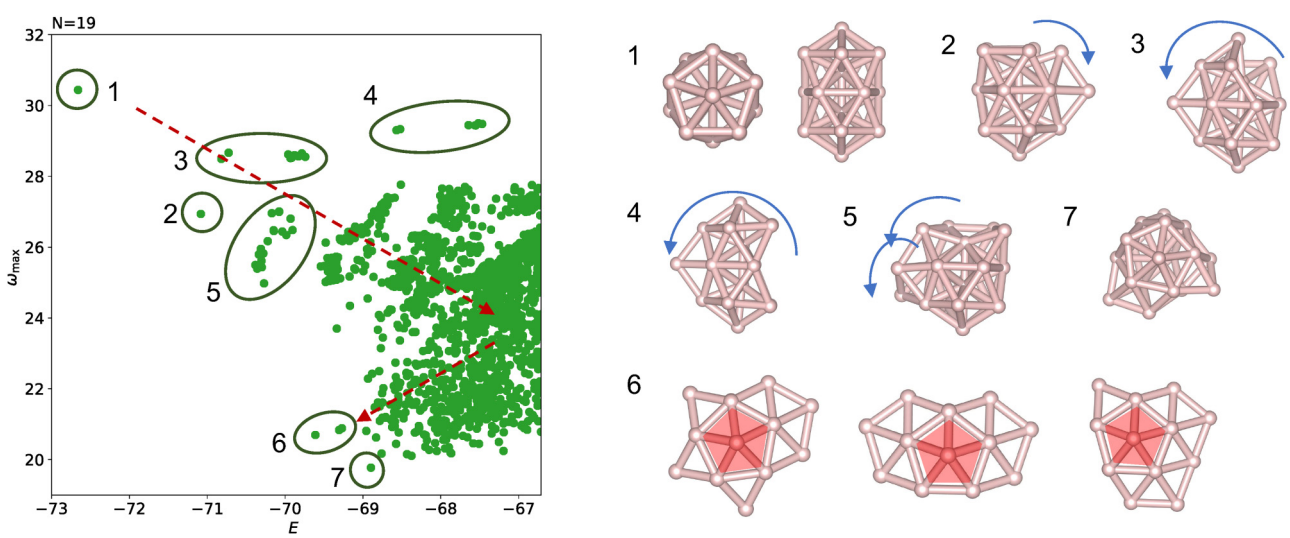

FIG. 5. (Left) The distribution of ω_{max} versus the total energy of E for the 2000 lowest energy structures with $N = 19$. The plotted points are classed into seven groups, where the group 6 includes three points. (Right) The illustration of metastable structures of groups 1–7, where the group 6 structures have a decahedron (colored red). The arrows indicate the atomic movements from the group 1 structure. The dashed arrows (left) indicate a potential pathway of the structural transformation from the group 1 to group 6.

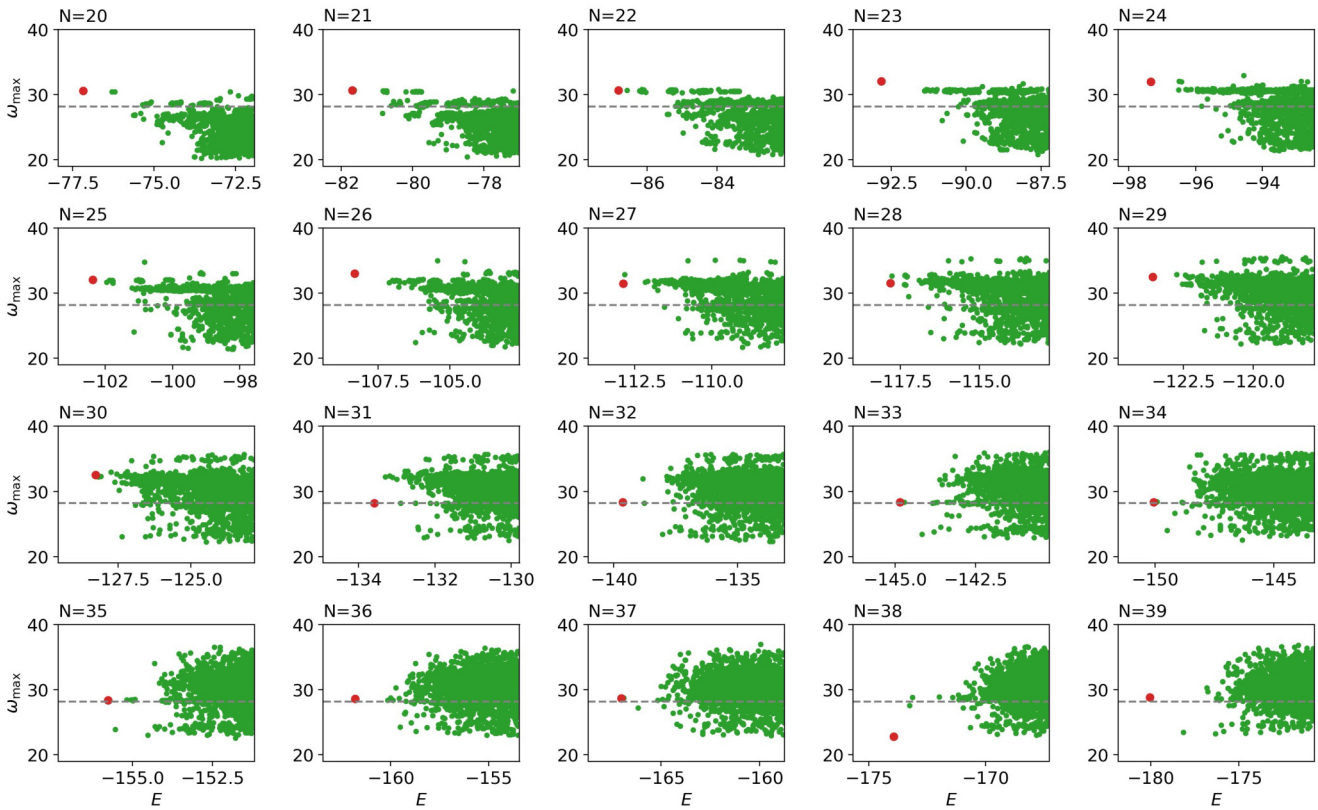

FIG. 6. The distribution of ω_{max} versus the total energy of E for the 2000 lowest energy structures with $N = 20$–39. The data of the lowest energy structure are indicated by a large circle (colored red). The dashed line indicates the ω_{max}^{fcc}.

of the group 6, implying that more than 5A (rather than 3A) is needed, as indicated by dashed arrows in Fig. 5. However, the exact determination of the barrier height requires a comprehensive search for the transition states and a construction of the disconnectivity graph [17], which is beyond the scope of the present work.

It is interesting that when the metastable structures differ strongly in geometry, those are located at different region in the E-ω_{max} plane, as shown in Fig. 5. This allows us to study the evolution of the cluster geometry with the size N. Figure 6 shows how the distribution of ω_{max} evolves within the range of $20 \leqslant N \leqslant 39$. When $20 \leqslant N \leqslant 30$, the distribution of ω_{max} is similar to that for the case of $N = 19$: the lowest energy structure has a relatively high value of ω_{max}, while some metastable structures have relatively small values of $\omega_{max} \simeq 22$. The former structures are constructed by adding atoms to the surface region of the lowest energy structure of $N = 19$, i.e., a double icosahedron, whereas the latter structures consist of decahedra. When N is increased to 31, the ω_{max} of the lowest energy structure becomes small ($\omega_{max} \simeq 28$), implying that the number of decahedra overcomes that of icosahedra. For $N \geqslant 32$, a strong distribution around $\omega_{max} = 32$ is smeared out, and the distribution of ω_{max} tends to be symmetric around $\omega_{max} = 30$. In the E-ω_{max} plane, islands evolve for low ω_{max} when N is increased, producing the octahedral structure at $N = 38$. For $N = 39$, the lowest energy structure ($\omega_{max} = 28.8$) is constructed from a decahedron surrounded by five decahedra, whereas the second lowest energy structure ($\omega_{max} = 23.5$) is constructed by adding an atom to the $N = 38$ octahedral structure. The energy barrier hight between them is estimated to be more than 5A rather than 2A, by assuming that there are relevant transition states in the continent of high energy states. In this way, the construction of the E-ω_{max} map is a useful method to understand the transformation between metastable structures.

The structural transition from the icosahedral to decahedral structures has been discussed in the literature. Deaven *et al.* identified a significant change in the one-particle energy distribution [14]: The peak of the lowest one-particle energy shifts dramatically from $\varepsilon_i \simeq -6.5$ at $N = 30$ to $\varepsilon_i \simeq -7$ at $N = 31$. On the other hand, Raoult *et al.* [12] and Shao *et al.* [25] showed that the structural transition to the decahedral structure occurs at $N > 1000$ by performing the total energy calculations. The present calculations suggest that the profile of the ω_{max} distribution is quite different across $N = 31$. We expect that the systematic calculations of the ω_{max} distribution for large N enable us to understand the structural transitions (from the icosahedral to decahedral, and from the decahedral to fcc structures as well).

IV. CONCLUSION

In conclusion, we studied the N dependence of the total energy E and the maximum frequency ω_{max} of the LJ clusters with the size up to $N = 1610$. The ω_{max} reflects the atomic vibrations localized at the core region, and the magnitude of ω_{max} is significantly small when the core geometry is different from an icosahedron (e.g., $N = 38$, 75–77, 98, and 102–104).

The $\omega_{\max}$ also reflects the vacancy formation at the core and the structural transition from icosahedra to decahedra for large N. Based on the relationship between the E and $\omega_{\max}$ for the cases of $19 \leqslant N \leqslant 39$, we created the metastability map that can provide both transformation pathways between different structures and an estimation of the energy barrier height. For a clarity, the strategy for creating the metastability map is summarized as follows: (1) Visualize the geometry of all clusters forming an island in Fig. 5, where the VESTA software [39] was used in the present work; (2) partition into several groups with similar geometries; and (3) analyze the trend of metastability map. Note that the strategy (2) may be done more efficiently by using machine learning approaches. The strategy (3) will include a rough estimation of the energy barriers between different structures (as discussed in Fig. 6) and a detailed analysis of the structural transformation. Note also that a construction of the disconnectivity graph is necessary to estimate the exact value of the barrier height [29,30].

We believe that the combination of the maximum frequency and the total energy would provide an interesting aspect for understanding the metastability of clusters. We hope that the $\omega_{\max}$-based approach is applied to study the metastability of more realistic systems including metallic and semiconducting clusters by using accurate potentials. On the other hand, the allotropes of fullerene molecules will show different N dependence of $\omega_{\max}$ because of the hollow spherical structures.

ACKNOWLEDGMENTS

This work was supported by JSPS KAKENHI (Grant No. 21K04628). The computation was carried out using the facilities of the Supercomputer Center, the Institute for Solid State Physics, the University of Tokyo, and using the supercomputer "Flow" at Information Technology Center, Nagoya University.

[1] B. Wang, J. Zhao, X. Chen, D. Shi, and G. Wang, Atomic structures and covalent-to-metallic transition of lead clusters Pb_n ($n = 2$–22), Phys. Rev. A **71**, 033201 (2005).

[2] J. P. K. Doye, Lead clusters: Different potentials, different structures, Comput. Mater. Sci. **35**, 227 (2006).

[3] H. Li, Y. Ji, F. Wang, S. F. Li, Q. Sun, and Y. Jia, Abinitio study of larger Pb_n clusters stabilized by Pb_7 units possessing significant covalent bonding, Phys. Rev. B **83**, 075429 (2011).

[4] Q. L. Lu, Q. Q. Luo, L. L. Chen, and J. G. Wan, Structural and magnetic properties of Ni_n ($n = 2$–21) clusters, Eur. Phys. J. D **61**, 389 (2011).

[5] D. Jiang and M. Walter, Au_{40}: A large tetrahedral magic cluster, Phys. Rev. B **84**, 193402 (2011).

[6] A. H. Larsen, J. Kleis, K. S. Thygesen, J. K. Nørskov, and K. W. Jacobsen, Electronic shell structure and chemisorption on gold nanoparticles, Phys. Rev. B **84**, 245429 (2011).

[7] M. J. Piotrowski, P. Piquini, and J. L. F. Da Silva, Density functional theory investigation of $3d$, $4d$, and $5d$ 13-atom metal clusters, Phys. Rev. B **81**, 155446 (2010).

[8] X. Wu and Y. Sun, Stable structures and potential energy surface of the metallic clusters: Ni, Cu, Ag, Au, Pd, and Pt, J. Nanopart. Res. **19**, 201 (2017).

[9] F. Baletto and R. Ferrando, Structural properties of nanoclusters: Energetic, thermodynamic, and kinetic effects, Rev. Mod. Phys. **77**, 371 (2005).

[10] S. Zhou, M. Zhao, T.-H. Yang, and Y. Xia, Decahedral nanocrystals of noble metals: Synthesis, characterization, and applications, Mater. Today **22**, 108 (2019).

[11] J. A. Northby, Structure and binding of Lennard-Jones clusters: $13 \leqslant N \leqslant 147$, J. Chem. Phys. **87**, 6166 (1987).

[12] B. Raoult, J. Farges, M. F. De Feraudy, and G. Torchet, Comparison between icosahedral, decahedral and crystalline Lennard-Jones models containing 500 to 6000 atoms, Phil. Mag. B **60**, 881 (1989).

[13] G. L. Xue, Improvement on the Northby algorithm for molecular conformation: Better solutions, J. Global Optimization **4**, 425 (1994).

[14] D. M. Deaven, N. Tit, J. R. Morris, and K. M. Ho, Structural optimization of Lennard-Jones clusters by a genetic algorithm, Chem. Phys. Lett. **256**, 195 (1996).

[15] D. J. Wales and J. P. K. Doye, Global optimization by basin-hopping and the lowest energy structures of Lennard-Jones clusters containing up to 110 atoms, J. Phys. Chem. A **101**, 5111 (1997).

[16] R. H. Leary and J. P. K. Doye, Tetrahedral global minimum for the 98-atom Lennard-Jones cluster, Phys. Rev. E **60**, R6320(R) (1999).

[17] J. P. K. Doye, M. A. Miller, and D. J. Wales, Evolution of the potential energy surface with size for Lennard-Jones clusters, J. Chem. Phys. **111**, 8417 (1999).

[18] F. Calvo, J. P. K. Doye, and D. J. Wales, Quantum partition functions from classical distributions: Application to rare-gas clusters, J. Chem. Phys. **114**, 7312 (2001).

[19] J. P. K. Doye and F. Calvo, Entropic effects on the structure of Lennard-Jones clusters, J. Chem. Phys. **116**, 8307 (2002).

[20] I. A. Solov'yov, A. V. Solov'yov, W. Greiner, A. Koshelev, and A. Shutovich, Cluster Growing Process and a Sequence of Magic Numbers, Phys. Rev. Lett. **90**, 053401 (2003).

[21] W. Polak and A. Patrykiejew, Local structures in medium-sized Lennard-Jones clusters: Monte Carlo simulations, Phys. Rev. B **67**, 115402 (2003).

[22] Y. Xiang, H. Jiang, W. Cai and X. Shao, An efficient method based on lattice construction and the genetic algorithm for optimization of large Lennard-Jones clusters, J. Phys. Chem. A **108**, 3586 (2004).

[23] Y. Xiang, L. Cheng, W. Cai, and X. Shao, Structural distribution of Lennard-Jones clusters containing 562 to 1000 atoms, J. Phys. Chem. A **108**, 9516 (2004).

[24] X. Shao, Y. Xiang, and W. Cai, Formation of the central vacancy in icosahedral Lennard-Jones clusters, Chem. Phys. **305**, 69 (2004).

[25] X. Shao, Y. Xiang, and W. Cai, Structural transition from icosahedra to decahedra of large Lennard-Jones clusters, J. Phys. Chem. A **109**, 5193 (2005).

[26] E. G. Noya and J. P. K. Doye, Structural transitions in the 309-atom magic number Lennard-Jones cluster, J. Chem. Phys. **124**, 104503 (2006).

[27] Z. Yang and L.-H. Tang, Coordination motifs and large-scale structural organization in atomic clusters, Phys. Rev. B **79**, 045402 (2009).

[28] S. Ono, Magic numbers for vibrational frequency of charged particles on a sphere, Phys. Rev. B **104**, 094105 (2021).

[29] O. M. Becker and M. Karplus, The topology of multidimensional potential energy surfaces: Theory and application to peptide structure and kinetics, J. Chem. Phys. **106**, 1495 (1997).

[30] D. J. Wales, M. A. Miller, and T. R. Walsh, Archetypal energy landscapes, Nature (London) **394**, 758 (1998).

[31] D. S. De, B. Schaefer, B. von Issendorff, and S. Goedecker, Nonexistence of the decahedral $Si_{20}H_{20}$ cage: Levinthal's paradox revisited, Phys. Rev. B **101**, 214303 (2020).

[32] B. W. B. Shires and C. J. Pickard, Visualizing Energy Landscapes Through Manifold Learning, Phys. Rev. X **11**, 041026 (2021).

[33] J. M. Ziman, *Electrons and Phonons* (Oxford University Press, New York, 1960).

[34] N. W. Ashcroft, N. D. Mermin, and D. Wei, *Solid State Physics* (Cengage, Boston, 2016).

[35] http://www-wales.ch.cam.ac.uk/CCD.html.

[36] https://chinfo.nankai.edu.cn/labintro_e.html.

[37] W. M. Press, B. P. Flannery, S. A. Teukolsky, and W. T. Vetterling, *Numerical Recipes in Fortran 90: The Art of Parallel Scientific Computing* (Cambridge University Press, Cambridge, 1996).

[38] S. Ono and T. Ito, Theory of dynamical stability for two- and three-dimensional Lennard-Jones crystals, Phys. Rev. B **103**, 075406 (2021).

[39] K. Momma and F. Izumi, VESTA 3 for three-dimensional visualization of crystal, volumetric and morphology data, J. Appl. Crystallogr. **44**, 1272 (2011).